ACS Catalysis

Research Article

pubs.acs.org/acscatalysis

Decoupling the Geometric Parameters of Shape-Controlled Pd Nanocatalysts

Moitree Laskar and Sara E. Skrabalak*

Department of Chemistry, Indiana University, 800 E. Kirkwood Avenue, Bloomington, Indiana 47405, United States

Supporting Information

ABSTRACT: The structural features of metal nanoparticles such as crystallite size and shape are important to catalytic activity and selectivity. Thus, correlating the performance of metal nanocatalysts to these structural features is important to understanding and designing better catalysts. In this paper, the size and shape effects of Pd nanocrystals are examined as they are applied as semihydrogenation catalysts. Seed-mediated growth methods were used to achieve samples composed of different-sized {100}-terminated Pd nanocubes and {111}-terminated Pd nanoctahedra, which served as model systems to evaluate the role of surface structure to activity and selectivity. The size of the nanocrystals was easily tuned by controlling the amount of metal deposited per seed. The selection of capping agent provided a means of manipulating the final shape of the nanocrystals. The catalysis results from this study will facilitate the decoupling of the size and shape contributions to the geometric parameters of Pd nanocatalysts.

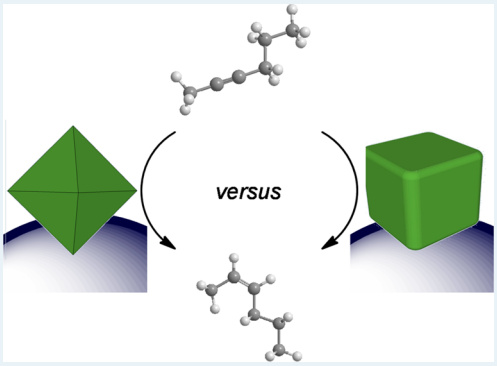

KEYWORDS: *Pd nanocubes, Pd nanoctahedra, nanocatalyst, geometric parameter, size effect, shape effect*

INTRODUCTION

Because of their increased surface-to-volume ratio with decreasing size, nanoparticles are promising platforms for heterogeneous catalysis.[1,2] Industrial processes in food processing,[3,4] drug delivery,[5] textile industries,[3,6] petroleum refining,[7] and environmental remediation[8] use metals in a finely divided state as effective catalysts. Importantly, the activity and selectivity provided by nanoparticulate catalysts can be enhanced through the use of size- and shape-controlled nanocrystals, which provide means to manipulate the geometric and electronic parameters governing surface−adsorbate interactions and, thus, catalytic performance.[9−15] This manuscript examines the geometric parameters of size- and shape-controlled Pd nanocrystals as they are applied as selective hydrogenation catalysts. {111}-terminated Pd octahedra were found to be more active than {100}-terminated Pd nanocubes with similar surface areas. Moreover, the intrinsic catalytic activity of the Pd catalysts increased with increasing nanocrystal size, regardless of shape. This study is significant as the two main geometric parameters governing the performance of metal nanocatalysts—nanocrystal size and shape—are systematically decoupled for the first time. These findings should provide design criteria for metal catalysts in general.

Although the surface-to-volume ratio of nanoparticles increases with their decrease in size, the intrinsic catalytic activity (i.e., catalytic activity normalized to surface area) can stay the same, be enhanced, or decrease as a function of particle size. These possibilities can be accounted for by either a change in the electronic structure of metal nanoparticles at small sizes or a change in surface structure as a function of nanoparticle size. Changes in electronic structure can arise from strain and quantum size effects in which sufficiently small metal nanoparticles display nonmetallic behavior with the appearance of a band gap.[16,17] However, the Pd nanocrystals examined here are all >20 nm in size and outside of the size regime in which such changes in electronic structure would be anticipated. Second, changes in electronic structure can arise from atoms at the surfaces of nanoparticles having different environments, i.e., occupying face, edge, or corner sites.[11,18] Atoms situated at these various sites have different coordination numbers and, in turn, different surface energies, surface−adsorbate interaction strengths, and reactivity. The relative ratio of these sites changes as a function of nanoparticle size and is the origin of the size-dependent geometric effect for metal nanocatalysts, where the performance of a catalyst depends on the symmetry match between the adsorbates and surface sites available.[19] For example, Li et al. found that the reaction rate for the Suzuki coupling reaction between phenylboronic acid and iodobenzene increased as the Pd nanoparticle size decreased from 6.6 nm to 3.9 nm when all surface atoms were considered.[20] However, no trend with size was evident when the activity was normalized against the number of vertex and edge sites, eliminating the possibility of an electronic effect with size. These results indicate that the coupling reaction is favored at low coordinated edge and corner sites rather than the face atoms. There are also examples of catalytic processes that prefer

Received: November 14, 2013
Revised: February 2, 2014
Published: March 6, 2014

   dx.doi.org/10.1021/cs401064d | ACS Catal. 2014, 4, 1120−1128

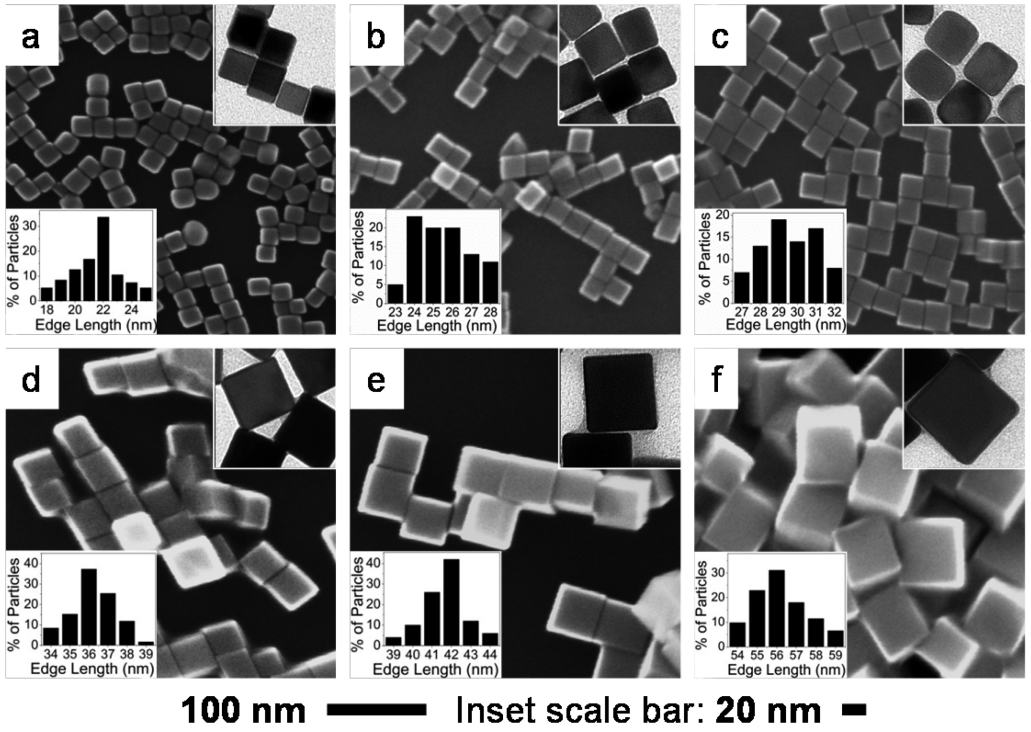

Figure 1. Scanning electron microscopy (SEM) images of Pd nanocubes with average edge lengths of (a) 22 nm, (b) 25 nm, (c) 30 nm, (d) 35 nm, (e) 42 nm, and (f) 56 nm. Transmission electron microscopy (TEM) images and size distributions are provided as insets.

face sites because of symmetry match between the functional groups of the reagent(s) and the surface atoms. In these cases, catalytic activity increases with larger particles. As a proof of this concept, Wilson et al. found that the hydrogenation rate of allyl alcohol was accelerated as the size of dendrimer-encapsulated quasi-spherical Pd nanoparticles increased from 1.5 nm to 1.9 nm.[21] A direct correlation between the hydrogenation rate and the number of face atoms on the particles lead them to conclude that the reaction favored face atoms, as opposed to edge or corner sites.

Of course, the relative ratio of different surface sites also depends on the shape of nanocrystals. For example, face-centered cubic (fcc) metals prepared as cubic nanoparticles will selectively express {100} facets, whereas octahedral nanoparticles will selectively express {111} facets. These facets have specific atomic arrangements, surface energies, and catalytic activity and selectivity. For example, a Pt(111) surface adsorbs oxygen atoms more efficiently than the Pt(100) surface. Thus, {111}-terminated Pt octahedra were shown to be more active electrocatalysts toward the oxygen reduction reaction than Pt nanocubes bound with {100} facets in the presence of perchloric acid as the electrolyte.[22] However, the activity of the {111}- and {100}-faceted nanoparticles was reversed when perchloric acid was substituted with sulfuric acid.[23] This observation was attributed to the greater adsorption of sulfate ions on the {111} facets of the particles, because of the 3-fold symmetry matching of sulfate ions with the atomic arrangement on the {111} facets. Also, Kiwi-Minsker and co-workers recently studied the structure sensitivity of alkynol hydrogenation on 6-nm and 18-nm Pd nanocubes as well as 31-nm Pd octahedra and 5.5-nm cuboctahedra.[24] They attributed the observed differences in performance to the presence of two types of active sites on these nanocrystals: one located on planes and the other located on edges.

In some of the examples discussed thus far, the nanoparticle surfaces are ligated, and these surface-bound groups can influence activity. Thus, groups have examined the removal of structure-directing agents and the subsequent use of the nanomaterials as catalysts to further substantiate the structure-dependent properties associated with shape-controlled nanocrystals. For example, Somorjai and co-workers used thermal oxidation−reduction treatments to remove poly(vinylpyrrolidone) from ∼9-nm Pt nanocubes, octahedra, and cuboctahedra.[25] These nanocrystals subsequently showed shape-dependent catalytic activities toward hydrogenation of unsaturated aldehydes. However, this shape-dependent activity might also arise from different amounts of residual Ag ions, which were required to obtain shape uniformity. Recently, Zaera and co-workers used similar cycles of annealing and oxidation−reduction to remove residual carbonaceous deposits from ∼5-nm Pt nanocubes and tetrahedra.[26] They found that {111}-terminated Pt tetrahedra were more effective at promoting the isomerization of *trans*- to *cis*-butene. These results again highlight the importance of geometric parameters to catalytic performance.

Although numerous groups have investigated the size and shape effects of nanoparticles on catalytic activity and selectivity, a systematic study that decouples these two geometric parameters has not been presented. However, by studying a series of size-controlled Pd nanocubes and octahedra as selective hydrogenation catalysts, the geometric parameters governed by nanocrystal size and shape are decoupled here for the first time. Two sets of experiments were necessary to achieve this goal. First, the size of the Pd nanocrystals was varied while holding the shape of the nanocrystals constant, to examine the effect of size on activity and selectivity in a semihydrogenation process. Second, by normalizing the number of surface atoms per particle, the catalytic activity and selectivity of differently shaped Pd nanocrystals (cube

dx.doi.org/10.1021/cs401064d | *ACS Catal.* 2014, 4, 1120−1128

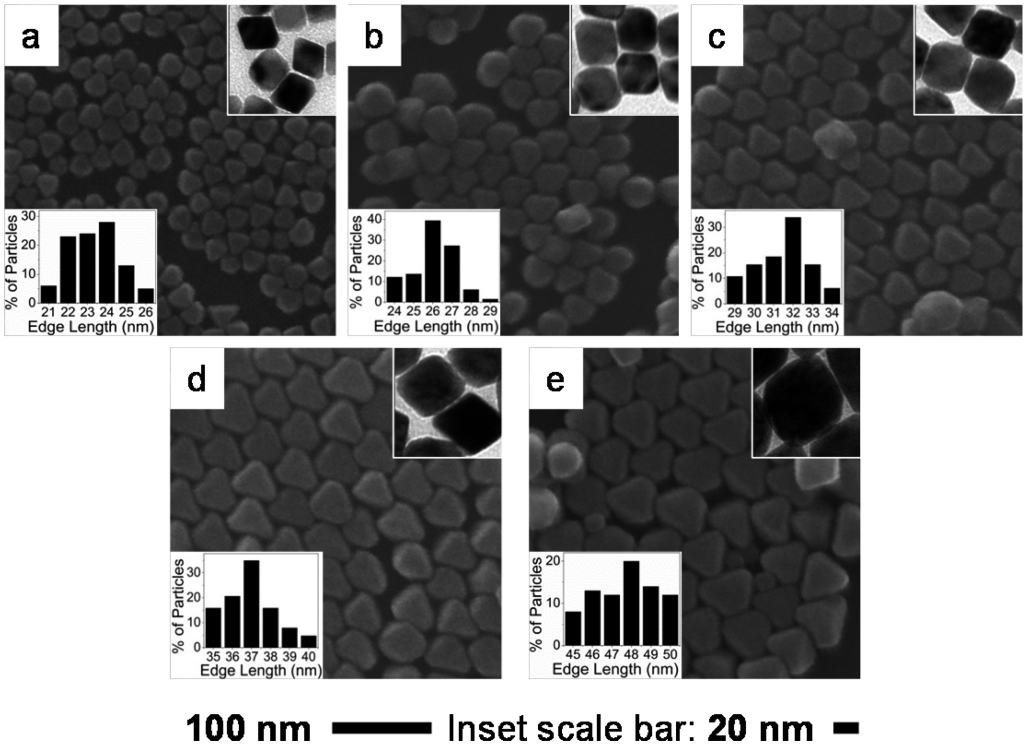

Figure 2. SEM images of Pd nanoctahedra with average edge lengths of (a) 23 nm, (b) 26 nm, (c) 32 nm, (d) 37 nm, and (e) 48 nm. TEM images and size distributions are provided as insets.

versus octahedra) were compared. As we found, the intrinsic catalytic activity of both Pd nanocubes and octahedra toward selective hydrogenation of 2-hexyne increased with increasing nanocrystal size. Moreover, octahedra were more-efficient catalysts, compared to nanocubes, when normalized to the total number the surface atoms. Significantly, these results provide criteria for the design of future catalysts based on size- and shape-controlled particles.

RESULTS AND DISCUSSION

Pd nanocubes with average edge lengths of 22 (±2) nm, 25 (±2) nm, 30 (±2) nm, 35 (±2) nm, 42 (±3) nm, and 56 (±4) nm and Pd nanoctahedra with average edge lengths of 23 (±1) nm, 26 (±1) nm, 32 (±2) nm, 37 (±2) nm, and 48 (±2) nm were prepared via modification of an established seed-mediated method.[27−29] Hexadecyltrimethylammonium bromide (CTAB) and hexadecyltrimethylammonium chloride (CTAC) were used as stabilizing agents, respectively. Details of the syntheses can be found in the Experimental Section and the Supporting Information. Scanning electron microscopy (SEM) and transmission electron microscopy (TEM) images of the nanocubes and octahedra, along with size histograms, are provided in Figures 1 and 2, respectively. To obtain the size histograms, the edge lengths of 100 nanocrystals were measured per sample from TEM images with omission of noncubic and non-octahedral particles from the size analysis. We note that Figure 2e indicates that spherical particles (~10%), along with the octahedra, are present in this sample. Otherwise, size and structural impurities are <1% in all other samples, indicating the ability to prepare high-quality shape-controlled nanocrystals. These higher-magnification images also indicate that the corners of the nanocubes and octahedra are slightly truncated; however, the extent of truncation is very similar for all samples and, hence, should influence their catalytic activities to similar degrees.

The size of the Pd nanocubes and octahedra were varied to examine the effect of nanocrystal size on catalytic activity and selectivity. These nanocrystals were used as catalysts for the selective hydrogenation of 2-hexyne as a model reaction. Selective hydrogenation reactions are important processes to the food, pharmaceutical, petrochemical, and polymer industries. Scheme 1 depicts the hydrogenation of 2-hexyne to *cis*-2-hexene, where the desired product is susceptible to isomerization and overhydrogenation to *trans*-2-hexene and hexane, respectively. Earlier studies by several groups have shown that selective hydrogenations of alkynes are surface-sensitive processes, and Pd catalysts are strongly selective toward partial hydrogenation.[18] This selectivity has been attributed to the difference in adsorption energies of alkyne versus alkane on Pd surfaces as well as the formation of subsurface carbon species.[18,30] Thus, this model reaction is a suitable platform for testing the role of different geometric parameters of Pd nanocrystals.

Scheme 1. Hydrogenation of 2-Hexyne

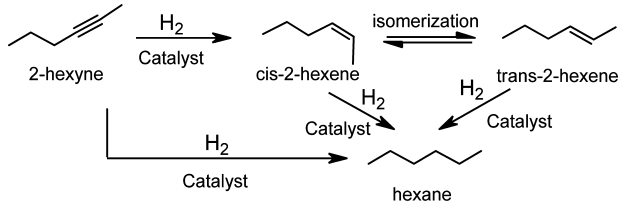

Prior to evaluation, the Pd nanocrystals were supported on TiO_2 to enhance their colloidal stability as unsupported nanocrystals agglomerated in solution and lead to decreased

dx.doi.org/10.1021/cs401064d | ACS Catal. 2014, 4, 1120−1128

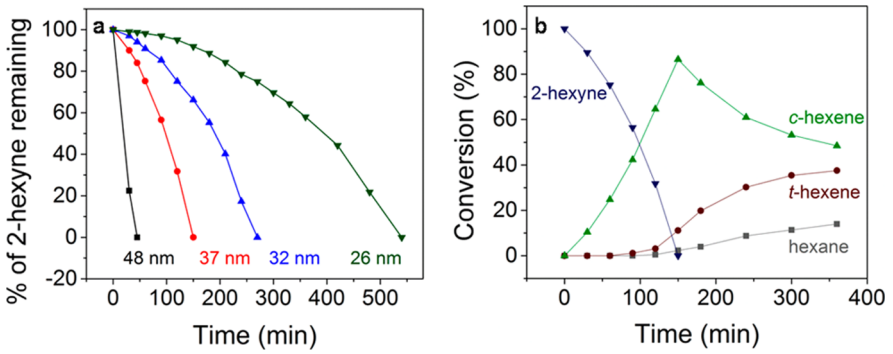

Figure 3. (a) Plot of the percentage of 2-hexyne remaining as a function of reaction time for Pd nanoctahedra with average edge lengths of 26, 32, 37, and 48 nm. (b) Plot of the relative conversion of reagent and products, as a function of reaction time for 37-nm Pd nanoctahedra.

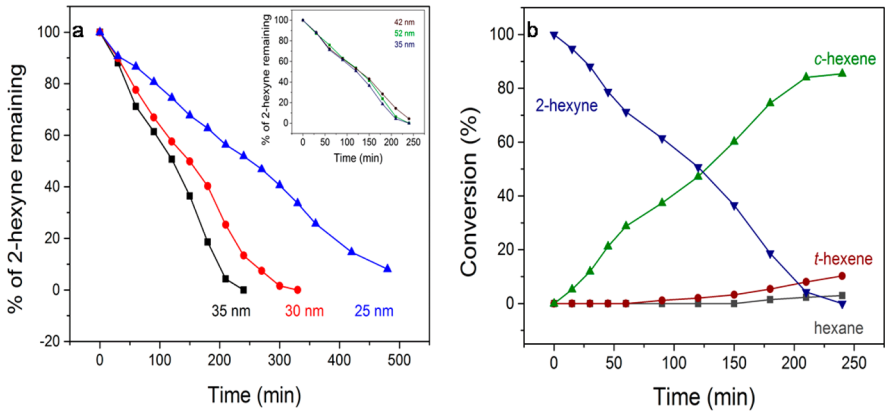

Figure 4. (a) Plot of the percentage of 2-hexyne remaining, as a function of reaction time for Pd nanocubes with average edge lengths of 25, 30, 35, 42, and 52 nm. (b) Plot of the relative conversion of reagent and products, as a function of reaction time for 35-nm Pd nanocubes.

catalytic activity. The Pd nanocrystals retained their original size and shape after being supported on TiO_2; however, some particle flocculation is also evident in all samples as observed by SEM (see Figures S1 and S2 in the Supporting Information). Although the TiO_2 support did not have any effect on the shape of the nanocrystals, X-ray photoelectron spectroscopy (XPS) revealed a 2.08 eV shift and a 2.42 eV shift to higher binding energy for the spin-coupling Pd 3d doublet, compared to that of the unsupported Pd nanocubes and nanoctahedra, respectively (see Figure S3 in the Supporting Information). The Pd 3d doublets were deconvoluted and higher-oxidation-state Pd was evident with the TiO_2-supported Pd nanocrystals (see Figure S4 in the Supporting Information). The presence of a higher oxidation state of Pd can be attributed to the electron transfer from the Pd surface to TiO_2.[31,32] Since the higher-oxidation-state Pd is present in similar amounts in both the Pd nanocubes and octahedra, this change in electronic structure is anticipated to influence catalytic activity similarly, regardless of shape. Otherwise, no significant difference in electronic structure was observed via XPS analysis when comparing the Pd nanocrystals of different sizes and shape (see Figure S5 in the Supporting Information), which was consistent with bulk Pd for the unsupported samples. This finding suggests that there are minimal changes in intrinsic strain when the size and shape of the nanocrystals were varied, which is consistent with their relatively large sizes. Powder X-ray diffraction (XRD) only yielded signals for TiO_2, because the Pd nanocrystal loading was too low for suitable diffraction (see Figure S6 in the Supporting Information). The supported, shape-controlled Pd nanocrystals were evaluated as catalysts for the hydrogenation of 2-hexyne under standard conditions as described in the Experimental Section. In the absence of Pd nanocrystals, the TiO_2 support is unable to facilitate hydrogenation of 2-hexyne in the presence of hydrogen (see Figure S7 in the Supporting Information).

To compare the intrinsic catalytic activity of the various shape-controlled Pd nanocrystals, the number of surface atoms relative to alkyne was held constant between experiments. This condition was met by adjusting the number of nanocrystals dispersed in solution in accordance with eq 1,[33] where the Pd loading on the TiO_2 support was measured using inductively coupled plasma mass spectrometry (ICP-MS) and TEM images were used to estimate the surface area of the nanocrystals from their size and shape,

$$N_A = An\rho \quad (1)$$

where N_A is the total surface atom, A the surface area, n the number of particles, and ρ the area density of surface atoms. The relative distribution of different types of surface atoms (face, edge, and corner) on the nanocrystals was then calculated using a method introduced by Van Hardeveld and Hartog based on the measured geometry.[34,35] Reaction aliquots were collected at regular intervals and were analyzed using gas chromatography–mass spectrometry (GC-MS).

Influence of Nanocrystal Size of Catalytic Activity and Selectivity. Size-dependent catalytic activities were observed for both the Pd nanocubes and nanoctahedra. Figure 3a shows the percentage of 2-hexyne consumed as a function of time with differently sized Pd nanoctahedra. The plot indicates that the intrinsic catalytic activity (i.e., normalized to the number of

dx.doi.org/10.1021/cs401064d | ACS Catal. 2014, 4, 1120–1128

Table 1. Edge Length, Calculated Surface Area, Turnover Frequency (TOF) (per Surface Atom), and Selectivity toward *cis*-2-Hexene of Pd Nanocubes and Nanooctahedra

shape	average edge length (nm)	surface area per particle (nm^2)	surface area:volume ratio	selectivity (%)	turnover frequency, TOF (s^{-1})
Pd nanocubes	25	3750	0.24	85.1 (±1.3)	1.7 (±0.8)
	30	5400	0.20	84.0 (±1.5)	2.6 (±0.6)
	35	7350	0.17	85.4 (±1.2)	3.7 (±0.7)
Pd nanooctahedra	26	2342	0.28	88.0 (±0.8)	1.6 (±0.7)
	32	3547	0.23	88.9 (±1.0)	3.2 (±0.5)
	37	4742	0.20	86.5 (±1.2)	5.9 (±0.4)
	48	7981	0.15	88.0 (±1.1)	19.3 (±0.8)

surface atoms) increases as the nanocrystal size increases. The fastest conversion was achieved with the largest nanooctahedra (edge length = 48 nm) analyzed. A similar trend was observed for Pd nanocubes with average edge lengths of 25 nm, 30 nm, and 35 nm, where the intrinsic catalytic activity again increased with crystal size (Figure 4a). However, Pd nanocubes with edge lengths greater than 35 nm did not show further increases in catalytic activity (inset of Figure 4a). Despite the fact that the catalytic activity increases with nanocrystal size, their selectivity toward *cis*-2-hexene at the point at which all 2-hexyne is consumed remained almost the same for all catalysts (Table 1). Figures 3b and 4b show representative plots of reactant-to-product transformations, as a function of reaction time. As observed in Figure 3b, selectivity decreases if the reaction proceeds beyond the point at which all 2-hexyne is consumed, with *cis*-2-hexene isomerizing to *trans*-2-hexene and complete hydrogenation achieved with the formation of hexane. This decrease in selectivity at longer times is observed with all the nanocatalysts studied. Although the Pd nanocubes and nanooctahedra display similar trends with regard to activity and selectivity, subtle differences in their catalytic behavior are also evident and will be discussed in detail shortly.

With homogeneous phase catalysts, comparisons of activity are often made by considering the turnover frequency (TOF), where the total number of molecules converted per second is normalized to the number of active sites (often the metal center of a complex). Considering the TOF for heterogeneous phase catalysts can also provide an easy means of comparing activity. In this case, TOF was considered as the total molecules of 2-hexyne converted per second (calculated from start to the time at which all 2-hexyne is consumed) by each Pd surface atom (calculated from eq 1) although we note that the active site likely contains more than one atom. The results are provided in Table 1, along with low standard deviations, and again confirm the size-dependent behavior of the shape-controlled nanocrystals, where catalytic activity increases with increase in crystal size. Although the TOFs are low compared to industrial catalysts, this comparison allows the trends in performance to be easily elucidated and will enable the contributions of nanocrystal size and shape to catalytic performance to be effectively decoupled.

Influence of Nanocrystal Shape on Catalytic Activity and Selectivity. In addition to size-dependent catalytic activity, the shape of the nanocrystals also played an important role. To compare the intrinsic activities of the Pd nanocubes to the Pd octahedra, the surface areas must be recalculated to consider the particle−support interaction. That is, when comparing supported nanocrystals of the same shape, we can assume that the relative number of facets exposed and available for catalysis does not change as a function of nanocrystal size. However, this assumption is not true when comparing supported nanocubes to supported octahedra, where 5 of 6 facets and 7 of 8 facets will be accessible, respectively. Considering this possibility, Pd nanocubes with an edge length of 25 nm and Pd octahedra with an edge length of 32 nm have similar surface areas available for catalysis (3125 nm^2 versus 3104 nm^2, respectively). Comparing these two samples allows for the shape-dependent catalytic activity to be elucidated, with the Pd nanooctahedra having a TOF almost two times (1.8 times) greater than that of the nanocubes. Though Pd nanooctahedra exhibited greater catalytic activity, the selectivity (88.9%) toward *cis*-2-hexene was comparable to the nanocubes (85.1%). However, we note that this analysis assumes similar degrees of particle flocculation for all TiO_2-supported samples.

Origin of Size- and Shape-Dependent Performance. As these results indicate, the size and shape of the Pd nanocrystals have a dramatic effect on activity; however, selectivity is not influenced in a significant way. The high affinity of alkynes to the Pd-surface accounts for the similar selectivity of these catalysts toward partial hydrogenation. As shown in Figure 3b and 4b, hydrogenation of the produced alkene to alkane is not observed until almost all alkyne is consumed. This observation is explained by the greater electronegativity of alkynes than alkenes, which results in stronger binding of the alkynes to the metal surface.[36] Thus, the generated alkene is displaced from its binding site as soon as it is formed by the remaining alkyne.[18] Readsorption of alkene followed by isomerization or complete hydrogenation cannot occur until the amount of 2-hexyne approaches zero and sites become available. This general trend of selectivity toward *cis*-2-hexene is observed for all the Pd catalysts studied in this document and is consistent with earlier experiments performed by Kiwi-Minsker and co-workers.[9,37]

Several reasons may account for the size-dependent catalytic behavior of these nanocrystals. First, the relative ratio of face atoms to edge and corner atoms changes with nanocrystal size. Specifically, the number of face atoms relative to corner and edge atoms increases as the crystal size increases (see Tables S1 and S2 in the Supporting Information for calculations of dispersion and different surface sites). However, the increase in the percentage of atoms in face sites is ∼0.5% when comparing the smallest to largest Pd nanocubes and ∼1.5% for Pd nanooctahedra while the overall activities increase by a factor of ∼2 for the Pd nanocubes and a factor of ∼12 for the Pd nanooctahedra. This back of the envelope calculation indicates that the increase in activity with size cannot be explained by the change in available face sites alone (see Table 1, as well as Tables S1 and S2 in the Supporting Information).

Another factor that may account for the enhanced catalytic performance of the larger particles is an ensemble effect. Such

an effect was previously described by Semagina et al. in their study of spherical Pd nanoparticles (with diameters of 6−14 nm) for the selective hydrogenation of 1-hexyne.[9] Specifically, they proposed that a minimum of five adjacent Pd atoms are required for 1-hexyne to adopt either the flat-lying π-adsorbed or di-σ-adsorbed mode required for hydrogenation on an fcc cuboctahedral crystal. Considering this simple geometric model, they found that the percentage of these multiatom reaction sites increases with increasing particle size; however, once a molecule adopts a position on a surface, the number of additional sites available may decrease by more than one, depending on the initial position selected. Thus, with larger particles, the probability of finding the required site for hydrogenation increases. In the case of the semihydrogenation of 2-hexyne, the parallel bridge mode[38] of adsorbed 2-hexyne is the precursor to *cis*-2-hexene in its flat-lying orientation, and this binding mode would occupy a cluster of surface Pd atoms similar to 1-hexyne adsorption on a Pd surface, as shown by Semagina.[9] Thus, the probability of finding the necessary ensemble of reactive sites is much greater for larger Pd nanocrystals than smaller ones and would account for the increase in the intrinsic catalytic activity of the Pd nanocubes and octahedra with size. At sufficiently large size, the probability of finding the necessary ensemble should no longer change appreciably and further increases in catalytic activity would not be anticipated, as observed with Pd nanocubes with edge lengths larger than 35 nm. Similar behavior would be anticipated with larger Pd octahedra; however, efforts to prepare such nanocrystals were unsuccessful.

The proposed ensemble effect with size-controlled Pd nanocrystals is further supported by examining the slopes of the different conversion curves. For example, in Figure 3a, the conversion curve associated with the 26-nm Pd octahedra displays an increase in activity at longer reaction times. In contrast, the conversion curve associated with the 48-nm Pd octahedra exhibits constant activity. The former behavior is consistent with a transition from a regime that is limited by the adsorption−desorption of reagent to a kinetic regime where the reaction itself is rate-determining. The latter behavior is consistent with the kinetic regime exclusively. Similar results have been observed by Rupprechter et al. in their study of Pd catalysts for the selective hydrogenation of 1,3-butadiene in which strongly bound butadiene inhibited hydrogen adsorption outside of the kinetic regime.[39,40] In the case of 2-hexyne hydrogenation, the strongly coordinating alkyne could inhibit hydrogen adsorption and account for the shape of the conversion curve when 26-nm Pd octahedra are used as catalysts. However, the amount of alkyne, relative to the Pd surface area, is the same regardless of the Pd nanocrystal size in these experiments. Thus, inhibition of hydrogen adsorption should be similarly likely with the 48 nm Pd octahedra, but such inhibition is not observed in the conversion curve. We attribute this observation again to an ensemble effect in which larger particles provide a greater percentage of the multiatom sites necessary for both alkyne and hydrogen adsorption.

Finally, the enhanced performance observed with the Pd octahedra compared to the Pd nanocubes with similar surface areas is consistent with previous reports. In particular, density functional theory (DFT) calculations performed by Medlin and Allendorf on the coordination of acetylene to different Pd surfaces suggest that variations in activity and selectivity might arise due to surface sensitive coordination of acetylene.[38] They proposed that acetylene coordinates to Pd(100) surfaces via four atoms in μ-bridging fashion, whereas di-σ bridging to one or two Pd atoms is suggested for Pd(111) surfaces. These differences in acetylene binding likely apply to other alkynes and suggest that alkynes are more strongly bound to Pd(100) surfaces than Pd(111) surfaces. Such differences might retard hydrogen binding or product desorption in the case of {100}-terminated Pd nanocubes. Thus, one would expect Pd nanocubes to exhibit a slower reaction rate for the hydrogenation of an alkyne, compared to the use of Pd octahedra, as is reported in this manuscript.

Influence of Surfactants on Catalytic Performance. These results indicate that catalytic performance is highly dependent on nanocrystal size and shape. However, the residual surfactants present on the surface of the nanocrystals may also contribute to the performance. For example, Kwon et al. demonstrated that capping agents can act as selectivity switches in alkyne hydrogenation reactions.[41] Their studies suggest that the addition of a primary alkyl amine can dramatically enhance the alkene selectivity from 0 to 90%. In the work presented here, the TiO_2-supported Pd nanocrystals were washed several times to remove as much CTAB or CTAC as possible. The Br^- 3d and Cl^- 2p peaks corresponding to the surfactants were not detected by XPS unless nearly 100 spectra were collected and summed and even then the signal-to-noise ratio is poor, making quantification challenging (see Figures S8 and S9 in the Supporting Information). Other efforts to completely remove the surfactants using either UV-ozone treatment[42,43] or oxygen plasma treatment[44] oxidized the Pd surfaces to PdO or decreased their stability, resulting in irreversible changes in nanocrystal shape. Given the low concentration of residual surfactant on the surfaces of the nanocrystals and the chemical similarity of the surfactants between all samples (all quaternary ammonium salts), we do not believe that the differences observed between the various samples can be explained by the presence of capping agents.

Post-Catalysis Characterization of TiO_2-Supported Pd Nanocrystals. Finally, the Pd nanocatalysts were characterized after use to identify whether or not any chemical or physical changes had occurred from use that may account for the observed activity and selectivity. The structural stability of the nanocrystals was verified by comparing SEM images of the particles before and after catalysis, with no significant changes in crystal size and shape observed (see insets in Figures S1 and S2 in the Supporting Information). The nanocrystals were also studied after catalysis using XPS, where it was observed that the Pd phase was shifted to lower binding energy. The Pd phase matches well with the unsupported Pd nanocrystals and suggests a change in the Pd nanocrystal−support interaction and possibly reduction of the Pd nanocrystal surface (see Figures S3c and S3d in the Supporting Information). However, the high-resolution scans also reveal that the smallest nanocrystals are partially oxidized after use, compared to the largest nanocrystals, although, before catalysis, no differences in the Pd regions were observed, irrespective of nanocrystal size and shape (see Figure S10 in the Supporting Information). This propensity toward oxidation may account for the diminished activity of the smallest nanocrystals with time. We also note that there is no evidence of Pd−Ti phase formation, which manifests in XPS spectra as shifts to higher binding energies occur for both Pd and Ti (see Figures S3e and S3f in the Supporting Information).[45,46] Such shifts were not observed in our samples after catalysis. When the TiO_2-supported nanocrystals were sputtered using a 1 keV argon ion beam for 1 min,

dx.doi.org/10.1021/cs401064d | *ACS Catal.* 2014, 4, 1120−1128

the higher oxidation component of the Pd signal decreases but no significant change is observed in the Ti region (see Figure S11 in the Supporting Information). This finding further corroborates that a Pd−Ti phase is not forming.[46]

CONCLUSIONS

In summary, the experimental results demonstrate that changing the size of the nanocrystals, irrespective of their shape, influences their catalytic activity. The activity increases as the size increases. As catalysis was performed with nanocrystals with same shape (Pd nanocubes or nanoctahedra) but various sizes, this result suggests that hydrogenation of alkynes is preferred on the face atoms rather than edges and corner atoms of these crystals. As alkyne hydrogenation prefers face atoms, this reaction was also analyzed as a function of nanocrystal shape (Pd nanocubes versus Pd nanoctahedra) with similar surface area. The difference in the surface atomic arrangements results in different binding of alkynes, where the Pd(100) surface binds alkynes more strongly than that of the Pd(111) surface. This variation in binding energy results in slower catalytic activity for {100}-terminated Pd nanocubes than with {111}-terminated Pd nanoctahedra. These results indicate that the geometric size effect can be decoupled from the geometric shape effect by keeping the nanocrystal shape constant and vice versa. Although demonstrated in a model system, these principles should extend to any surface sensitive catalytic reaction, where both nanocrystal size and shape must be preciously controlled to achieve maximum activity and selectivity.

EXPERIMENTAL SECTION

I. Chemicals. All chemicals were used as purchased without further purification. Potassium tetrachloropalladate (K_2PdCl_4), palladium(II) chloride ($PdCl_2$, 99.98%), L-ascorbic acid ($C_6H_8O_6$, AA, 99%), hexadecyltrimethylammonium bromide ($C_{19}H_{42}NBr$, CTAB, 98%), hexadecyltrimethylammonium chloride ($C_{19}H_{42}NCl$, CTAC, 25 wt % solution in water), titanium(IV) oxide (TiO_2, anatase, 325 mesh, ≥ 99% metals basis), and 2-hexyne (C_6H_{10}, 99%) were purchased from Sigma−Aldrich. Citric acid anhydrous ($C_6H_8O_7$) was obtained from VWR International. A 10 mM H_2PdCl_4 solution was prepared by stirring 0.0177 g $PdCl_2$ (10 mM) in 10 mL HCl (20 mM) at 40 °C for 1 h. Nanopure water with resistivity 18 MΩ cm (Millipore) was used in all experiments.

II. Synthesis of Nanostructures. *IIa. Synthesis of Size-Controlled Pd Nanocubes.* Pd nanocubes of various sizes were prepared following a previously reported seed-mediated growth method with slight modification.[27,28] In this procedure, smaller Pd nanocubes (~22 nm in edge length) were prepared, which were used as seeds for the further deposition of Pd to obtain bigger nanocubes.

IIa.1. Synthesis of Cubic Pd Seed (Edge Length: ~22 nm). In a typical synthesis, cubic Pd seeds with an edge length of ~22 nm were prepared by adding 0.5 mL of a 10 mM aqueous solution of H_2PdCl_4 to 10 mL of an aqueous 12.5 mM solution of CTAB under stirring at 600 rpm at 95 °C. After 5 min, 0.08 mL of a freshly prepared 100 mM aqueous solution of AA was added. The reaction was allowed to proceed for 30 min and was stopped by cooling to room temperature. Seeds were preserved at 40 °C for future use. Larger nanocubes were prepared using these smaller Pd nanocubes as seeds without further modification. Seed solutions were collected for characterization by centrifugation at 15 000 rpm for 15 min. The supernatant was removed and the particles were dispersed in water. This process of washing was repeated twice to remove most of the surfactants. All other nanocrystals were collected in similar fashion for characterization, unless otherwise noted. To stabilize the nanocrystals on TiO_2, all the samples were used as synthesized without any modification (see section III).

IIa.2. Synthesis of Pd Nanocubes (Edge Lengths: ~25, 30, 35, 42, and 56 nm). 0.125 mL of a 10 mM aqueous solution of H_2PdCl_4 was added to 5 mL of a 50 mM aqueous CTAB solution and kept at 40 °C. A 0.40 mL aliquot of the 22 nm cubic Pd seed solution was injected to obtain ~35 nm cubes. Cubes ranging from 42 and 56 nm can be obtained by varying the amount of Pd seed solution to 0.20 and 0.10 mL, respectively. Finally, 0.025 mL of a 100 mM aqueous AA solution was added, mixed thoroughly by shaking, and allowed to heat at 40 °C for 14 h. Twenty-five nanometer (25-nm) and 30-nm nanocubes were obtained by varying the amount of H_2PdCl_4 solution, keeping all other conditions similar to the one that gave 35-nm nanocubes. Specifically, 0.05 mL of 10 mM H_2PdCl_4 solution yielded 30-nm cubes, and 25-nm cubes were obtained using 0.02 mL of 10 mM H_2PdCl_4 solution.

IIb. Synthesis of Size-Controlled Pd Nanoctahedra. Pd nanoctahedra were prepared via a seeded-growth method similar to the one used to prepare Pd nanocubes. For the preparation of Pd nanoctahedra, initially smaller Pd octahedra were prepared, which were used as seeds and more Pd was deposited on top of them to grow bigger Pd nanoctahedra.

IIb.1. Synthesis of Octahedral Pd Seed (Edge Length: ~23 nm). The synthesis of Pd nanoctahedra was achieved by a reported method.[29] Two milliliters (2 mL) of a 156 mM aqueous citric acid solution and 2 mL of a 170 mM of aqueous AA solution was added to 4 mL of a 200 mM aqueous CTAC solution and stirred at 100 °C. Three milliliters (3 mL) of a 68 mM aqueous K_2PdCl_4 solution was added to the above mixture and kept at 100 °C for 3 h. This solution was diluted 100 times for further use as seed.

IIb.2. Synthesis of Pd Nanoctahedra (Edge Lengths: ~26, 32, 37, and 48 nm). Two milliliters (2 mL) of a 156 mM aqueous citric acid solution was added to 5 mL of a 100 mM aqueous CTAC solution. One milliliter (1 mL) of the 100 times diluted 23 nm Pd nanoctahedra seed solution was added to the above mixture, followed by the addition of 1 mL of an aqueous 5 mM K_2PdCl_4 solution. The reaction mixture was thoroughly mixed by inversion and kept at 70 °C for 20 h to synthesize 37-nm Pd nanoctahedra. Pd nanoctahedra having an edge length of ~32 and 26 nm can be obtained by varying the CTAC concentration to 150 mM and 200 mM, respectively. Pd octahedra having edge length of 48 nm were obtained by increasing the amount of Pd precursor and keeping all other conditions the same as the one that produces 37 nm octahedra. A quantity of 1.3 mL of 5 mM K_2PdCl_4 produced 48-nm octahedra.

III. Supporting Pd Nanocrystals on TiO_2. The nanocrystals were supported on TiO_2 by stirring a slurry of TiO_2 in 120 mL of water and a solution of as-prepared nanocrystals overnight at room temperature. A quantity of 0.12 mM of TiO_2 was added to appropriate amount of Pd nanocrystal solution containing ~2.5×10^{16} surface atoms (99.39×10^{-6} g for 25-nm Pd nanocubes, 116.36×10^{-6} g for 30-nm Pd nanocubes, 137.34×10^{-6} g for 35-nm Pd nanocubes, 165.86×10^{-6} g for 42-nm Pd nanocubes, and 203.92×10^{-6} g for 56-nm Pd nanocubes and 72.16×10^{-6} g for 26-nm Pd nanoctahedra, 87.15×10^{-6} g for 32-nm Pd nanoctahedra, 102.36×10^{-6} g for 37-nm Pd nanoctahedra, and 131.53×10^{-6} g for 48-nm Pd nanoctahedra). The samples were collected by centrifugation at 3900 rpm for 90 min. The supernatant were discarded, and the TiO_2 supported nanocrystals were dried in a vacuum oven at room temperature.

IV. Hydrogenation of 2-Hexyne. In a typical reaction, a 250-mL three-necked round-bottom flask, equipped with a stir bar, was evacuated for 30 min. The flask was filled with hydrogen using a balloon. Next, a mixture of supported Pd nanocrystals dispersed in 20 mL of ethanol was introduced in the reaction vessel along with 0.25 mL of 2-hexyne. Aliquots were collected at regular intervals and centrifuged at 15 000 rpm for 15 min to remove the TiO_2-supported metals as nonvolatile substance may contaminate the column of gas chromatograph used to analyze the sample. The products from the catalysis reactions were separated and analyzed using an Agilent Model 6890 gas chromatograph and an Agilent Model 5973 inert mass-selective detector.

V. Characterization of Nanocrystals. Images of the nanocrystals were taken via a JEOL Model JEM 1010 transmission electron microscope (TEM) at 80 kV with a ROM CCD camera and on a FEI

Quanta 600F environmental scanning electron microscope (SEM) operated at 30 kV and a spot size of 3. Samples for TEM analysis were prepared by drop-casting a dispersed particle solution onto a carbon-coated copper grid and then washing the grid twice with water. Samples for SEM were prepared by drop-casting a dispersed particle solution onto a silicon wafer and then washing the wafer three times with methanol after initial solvent evaporation. The Pd concentrations in all of the samples prepared above were measured using Perkin–Elmer ELAN DRCII ICP-MS. Pd nanocrystals were digested in aqua regia and standard solutions of known Pd concentrations were used to obtain the correct concentration. The products from the catalysis reactions were analyzed using an Agilent Model 6890 gas chromatograph and an Agilent Model 5973 inert mass-selective detector. Harrick Plasma (PDC-32G) was used to treat the samples for oxygen-plasma cleaning and for UV-ozone treatment, the samples were irradiated with a 6 W mercury lamp emitting at 185 and 257 nm. XPS spectra of the Pd nanocrystals were collected using a PHI Versa Probe II scanning X-ray microprobe under ultrahigh vacuum conditions and with a monochromatic Al Kα X-ray source. To compensate any charging effect, the C 1s peak was calibrated at 284.8 eV and was used as an internal standard. Powder X-ray diffraction (XRD) was performed on a Panalytical Empyrean instrument with Cu Kα radiation.

■ ASSOCIATED CONTENT

Supporting Information

Discussion on nanocrystal size optimization, SEM images of TiO_2-supported Pd nanocubes and nanoctahedra, XPS data of TiO_2-supported and unsupported Pd nanocubes and nanoctahedra, and powder X-ray diffraction data of TiO_2-supported Pd octahedra. This material is available free of charge via the Internet at http://pubs.acs.org.

■ AUTHOR INFORMATION

Corresponding Author

*E-mail: sskrabal@indiana.edu.

Author Contributions

The manuscript was written through contributions of all authors. All authors have given approval to the final version of the manuscript.

Funding

Seed funding for this research has been provided by start-up funds and a Dean's Fellowship from Indiana University-Bloomington, the Alfred P. Sloan Foundation, the Cottrell Scholar Program (Research Corporation) and is now supported by the U.S. Department of Energy (Basic Energy Sciences) through an Early Career Award Grant (No. 205883). Instrumentation has been made possible through NSF CRIF Grant No. 1048613 and NSF MRI Grant No. 1126394.

Notes

The authors declare no competing financial interest.

■ ACKNOWLEDGMENTS

We thank Prof. David P. Giedroc and John P. Lisher for their help with the ICP-MS instrument. We thank Dr. Yaroslav Lozovyy for his assistance with the XPS, Dennis Chen for his help in powder X-ray diffraction data collection, and Dr. Jonathan A. Karty for his help with the GC-MS instrument. We also want to thank the IU Nanoscale Characterization Facility for access to the necessary instrumentation.

■ REFERENCES

(1) Schauermann, S.; Nilius, N.; Shaikhutdinov, S.; Freund, H.-J. *Acc. Chem. Res.* **2013**, *46*, 1673–1681.
(2) Zaera, F. *ChemSusChem* **2013**, *6*, 1797–1820.
(3) Hajipour, M. J.; Fromm, K. M.; Akbar Ashkarran, A.; Jimenez de Aberasturi, D.; Ruiz de Larramendi, I.; Rojo, T.; Serpooshan, V.; Parak, W. J.; Mahmoudi, M. *Trends Biotechnol.* **2012**, *30*, 499–511.
(4) Zhang, H.; Toshima, N. *Catal. Sci. Technol.* **2013**, *3*, 268–278.
(5) De, J. W. H.; Borm, P. J. A. *Int. J. Nanomed.* **2008**, *3*, 133–149.
(6) Karst, D.; Yang, Y. *AATCC Rev.* **2006**, *6*, 44–48.
(7) Zaera, F. *Appl. Catal., A* **2002**, *229*, 75–91.
(8) Zhang, W.-x. *J. Nanopart. Res.* **2003**, *5*, 323–332.
(9) Semagina, N.; Renken, A.; Kiwi-Minsker, L. *J. Phys. Chem. C* **2007**, *111*, 13933–13937.
(10) Zhang, H.; Jin, M.; Xiong, Y.; Lim, B.; Xia, Y. *Acc. Chem. Res.* **2013**, *46*, 1783–1794.
(11) Semagina, N.; Kiwi-Minsker, L. *Catal. Rev.-Sci. Eng.* **2009**, *51*, 147–217.
(12) Tsung, C.-K.; Kuhn, J. N.; Huang, W.; Aliaga, C.; Hung, L.-I.; Somorjai, G. A.; Yang, P. *J. Am. Chem. Soc.* **2009**, *131*, 5816–5822.
(13) Knecht, M.; Pacardo, D. *Anal. Bioanal. Chem.* **2010**, *397*, 1137–1155.
(14) Roldan Cuenya, B. *Acc. Chem. Res.* **2012**, *46*, 1682–1691.
(15) An, K.; Somorjai, G. A. *ChemCatChem* **2012**, *4*, 1512–1524.
(16) Valden, M.; Lai, X.; Goodman, D. W. *Science* **1998**, *281*, 1647–1650.
(17) Valden, M.; Pak, S.; Lai, X.; Goodman, D. W. *Catal. Lett.* **1998**, *56*, 7–10.
(18) Molnár, Á.; Sárkány, A.; Varga, M. *J. Mol. Catal. A—Chem.* **2001**, *173*, 185–221.
(19) Semagina, N.; Renken, A.; Laub, D.; Kiwi-Minsker, L. *J. Catal.* **2007**, *246*, 308–314.
(20) Li, Y.; Boone, E.; El-Sayed, M. A. *Langmuir* **2002**, *18*, 4921–4925.
(21) Wilson, O. M.; Knecht, M. R.; Garcia-Martinez, J. C.; Crooks, R. M. *J. Am. Chem. Soc.* **2006**, *128*, 4510–4511.
(22) Markovic, N. M.; Adzic, R. R.; Cahan, B. D.; Yeager, E. B. *J. Electroanal. Chem.* **1994**, *377*, 249–259.
(23) Wang, C.; Daimon, H.; Onodera, T.; Koda, T.; Sun, S. *Angew. Chem., Int. Ed.* **2008**, *47*, 3588–3591.
(24) Crespo-Quesada, M.; Yarulin, A.; Jin, M.; Xia, Y.; Kiwi-Minsker, L. *J. Am. Chem. Soc.* **2011**, *133*, 12787–12794.
(25) Rioux, R. M.; Song, H.; Grass, M.; Habas, S.; Niesz, K.; Hoefelmeyer, J. D.; Yang, P.; Somorjai, G. A. *Top. Catal.* **2006**, *39*, 167–174.
(26) Lee, I.; Morales, R.; Albiter, M. A.; Zaera, F. *Proc. Natl. Acad. Sci. USA* **2008**, *105*, 15241–15246.
(27) Niu, W.; Li, Z.-Y.; Shi, L.; Liu, X.; Li, H.; Han, S.; Chen, J.; Xu, G. *Cryst. Growth Des.* **2008**, *8*, 4440–4444.
(28) Niu, W.; Zhang, L.; Xu, G. *ACS Nano* **2010**, *4*, 1987–1996.
(29) Hong, J. W.; Kim, D.; Lee, Y. W.; Kim, M.; Kang, S. W.; Han, S. W. *Angew. Chem., Int. Ed.* **2011**, *50*, 8876–8880.
(30) Teschner, D.; Borsodi, J.; Wootsch, A.; Révay, Z.; Hävecker, M.; Knop-Gericke, A.; Jackson, S. D.; Schlögl, R. *Science* **2008**, *320*, 86–89.
(31) Cai, Y.; Bai, Z.; Chintalapati, S.; Zeng, Q.; Feng, Y. P. *J. Chem. Phys.* **2013**, *138*, 154711.
(32) Mekasuwandumrong, O.; Phothakwanpracha, S.; Jongsomjit, B.; Shotipruk, A.; Panpranot, J. *Catal. Lett.* **2010**, *136*, 164–170.
(33) Wu, H.-L.; Tsai, H.-R.; Hung, Y.-T.; Lao, K.-U.; Liao, C.-W.; Chung, P.-J.; Huang, J.-S.; Chen, I. C.; Huang, M. H. *Inorg. Chem.* **2011**, *50*, 8106–8111.
(34) Van Hardeveld, R.; Hartog, F. *Surf. Sci.* **1969**, *15*, 189–230.
(35) Van Hardeveld, R.; Hartog, F. *Adv. Catal.* **1972**, *22*, 75–113.
(36) Zaera, F. *Chem. Rev.* **1995**, *95*, 2651–2693.
(37) Ruta, M.; Semagina, N.; Kiwi-Minsker, L. *J. Phys. Chem. C* **2008**, *112*, 13635–13641.
(38) Medlin, J. W.; Allendorf, M. D. *J. Phys. Chem. B* **2003**, *107*, 217–223.
(39) Silvestre-Albero, J.; Rupprechter, G.; Freund, H.-J. *Chem. Commun.* **2006**, 80–82.
(40) Silvestre-Albero, J.; Rupprechter, G.; Freund, H.-J. *J. Catal.* **2006**, *240*, 58–65.

(41) Kwon, S. G.; Krylova, G.; Sumer, A.; Schwartz, M. M.; Bunel, E. E.; Marshall, C. L.; Chattopadhyay, S.; Lee, B.; Jellinek, J.; Shevchenko, E. V. *Nano Lett.* **2012**, *12*, 5382−5388.
(42) Aliaga, C.; Park, J. Y.; Yamada, Y.; Lee, H. S.; Tsung, C.-K.; Yang, P.; Somorjai, G. A. *J. Phys. Chem. C* **2009**, *113*, 6150−6155.
(43) Crespo-Quesada, M.; Andanson, J.-M.; Yarulin, A.; Lim, B.; Xia, Y.; Kiwi-Minsker, L. *Langmuir* **2011**, *27*, 7909−7916.
(44) Gehl, B.; Frömsdorf, A.; Aleksandrovic, V.; Schmidt, T.; Pretorius, A.; Flege, J.-I.; Bernstorff, S.; Rosenauer, A.; Falta, J.; Weller, H.; Bäumer, M. *Adv. Funct. Mater.* **2008**, *18*, 2398−2410.
(45) Bzowski, A.; Sham, T. K. *Phys. Rev. B* **1993**, *48*, 7836−7840.
(46) Lisowski, W.; Keim, E. G.; Kaszkur, Z.; Berg, A. H. J.; Smithers, M. A. *Anal. Bioanal. Chem.* **2007**, *389*, 1489−1498.